Published by
NIGERIAN SOCIETY OF PHYSICAL SCIENCES
Available online @ https://journal.nsps.org.ng/index.php/jnsps

J. Nig. Soc. Phys. Sci. 2 (2020) 205–217

Journal of the Nigerian Society of Physical Sciences

Effect of benzophenone on the physicochemical properties of N-CNTs synthesized from 1-ferrocenylmethyl (2-methylimidazole) catalyst

Ayomide Hassan Labulo[a,*], Elijah Temitope Adesuji[a], Charles Ojiefoh Oseghale[a], Elias Emeka Elemike[b], Adamu Usman[a], Akinola Kehinde Akinola[c], Enock Olugbenga Dare[c]

[a]*Department of Chemistry, Federal University of Lafia, Lafia, Nasarawa State, Nigeria*
[b]*Department of Chemistry, Federal University of Petroleum, Nigeria*
[c]*Department of Chemistry Federal University of Agriculture, Abeokuta, Ogun State, Nigeria*

Abstract

Vertically-aligned nitrogen-doped carbon nanotubes (v-N-CNTs) were synthesized *via* the chemical vapour deposition (CVD) technique. 1-ferrocenylmethyl(2-methylimidazole) was employed as the source of the Fe catalyst and was dissolved in different ratios of acetonitrile/benzophenone feedstock which served as both the carbon, nitrogen, and oxygen sources. The morphological difference in N-CNTs was as a result of increased oxygen concentration in the reaction mix and not due to water vapour formation as observed in the oxygen-free experiment, indicating specifically, the impact of oxygen. Raman and X-ray photoelectron spectroscopy (XPS) revealed surface defects and grafting of oxygen functional groups on the sidewall of N-CNTs. The FTIR data showed little or no effect as oxygen concentration increases. XPS analysis detected the type of nitrogen species (*i.e.* pyridinic, pyrrolic, graphitic, or molecular nitrogen forms) incorporated in the N-CNT samples. Pyrrolic nitrogen was dominant and increased (from 8.6 to 11.8 at.%) as oxygen concentration increases in the reaction precursor. An increase in N content was observed with the introduction of a lower concentration of oxygen, followed by a gradual decrease at higher oxygen concentration. Our result suggested that effective control of the reactant mixtures can manipulate the morphology of N-CNTs.

DOI:10.46481/jnsps.2020.105

Keywords: Chemical vapour deposition, nitrogen-doped carbon nanotubes, 1-ferrocenylmethyl(2-methylimidazole), X-ray photoelectron spectroscopy

Article History :
Received: 11 May 2020
Received in revised form: 08 August 2020
Accepted for publication: 09 August 2020
Published: 15 November 2020

Communicated by: B. J. Falaye

1. Introduction

Vertically-aligned carbon nanotubes (v-CNTs) have been found to be fascinating for various range of applications, such as catalysis (as catalyst support) [1, 2, 3], electronics [4, 5, 7] and biological [8, 9, 10] devices. This is as a result of the controllable diameter and surface area of v-CNTs [11] which can be explored in the fabrication of materials of particular interest. The major drawbacks of v-CNTs are their low selectivity and reactivity at the surface. These drawbacks can be overcome by surface functionalization and nitrogen-doping which tailor their physicochemical properties [12]. Doping of CNTs

*Corresponding author tel. no: +234 8062295936
Email address: labulo@yahoo.com (Ayomide Hassan Labulo)

with heteroatoms, such as B, P, S and N, into the sp^2 carbon framework has been reported [13, 14, 15, 16]. These electron-rich atoms help fine-tune the electronic properties of CNTs [2]. Also, nitrogen incorporation into CNTs alters the wall thickness, crystallinity and diameter of CNTs [17]. The nitrogen embedded into CNTs can take various forms. The most common are graphitic-nitrogen, pyrrolic-nitrogen, pyridinic-nitrogen and molecular N_2 stuck in the interior of CNT structures [18, 19, 20]. The nitrogen composition largely depends on the solubility of nitrogen in the catalyst nanoparticle during the reaction at a specified temperature. It has been shown that the type and concentration of nitrogen obtained depend on the nature of the catalyst employed (*i.e.* ferrocene or ferrocenyl derivatives), synthetic temperature, gas flow rate and type of nitrogen-containing precursors [21, 22, 23].

Several methods have been employed in the synthesis of N-CNTs; namely arc-discharge [24], laser deposition [25] and chemical vapour deposition (CVD) [26]. Of these, the CVD technique has been the method commonly used for large-scale N-CNT synthesis [27]. However, the control of the reaction conditions in CVD technique is somewhat tricky, as catalyst poisoning due to limiting carbon diffusion rate and formation of amorphous carbon on Fe substrate surface is common [28, 29]. Many researchers have reported the introduction of oxygen [30], water [31, 32] and CO_2 [33], ethyl benzoate [34] among other reaction gases to improve N-CNTs quality and catalyst activity [35]. However, an excess level of oxygen-containing species could lead to N-CNTs etching [29, 32, 36]. Recently, Sakurai *et al*. [37] reported that the introduction of the oxygen-containing molecule (e.g. H_2O) during CVD synthesis enhanced the growth of CNTs and prolong catalyst lifetime at temperatures above 750 °C. This resulted in the removal of amorphous carbon through water vapour etching to give a graphitic nanostructured carbon network [26]. Fatuba *et al*. [38] also reported that the addition of oxygen-containing aromatic compounds (i.e. growth enhancer), such as methyl benzoate and benzaldehyde into the reaction mixture tailored the size and controlled the N-CNTs wall numbers and alignment [38]. The essential role of the growth enhancer compared to previously reported approach (such as H_2O), is to control the wall numbers, diameters and to reactivate catalyst particles [39, 40, 41].

In this study, we report for the first time, the use of benzophenone in the reactant mixture to modify N-CNTs growth and morphology. Benzophenone was also employed to improve the solubility of the ferrocenyl imidazolium catalyst in acetonitrile. We elucidate the effect of oxygen on the type of nitrogen incorporated in N-CNTs. The morphology, surface area and stability of N-CNTs were studied at varying oxygen concentration levels.

2. Experimental

2.1. Materials and characterization

Ferrocene (≥ 97%), ferrocenemethanol (98%), 2-methylimidazole (≥ 98.2%) and sodium borohydride (95%), potassium hydrogen phthalate (≥ 99.5%) were obtained from Sigma Aldrich Ltd. South Africa. Acetonitrile (HPLC grade, 99.9%), toluene (≥99.5%) and ethanol (98%) were purchased from Merck Chemicals South Africa. Nitric acid (55%) and sulphuric acid (98%) were purchased from Saarchem, South Africa. 10% Hydrogen in argon (purchased from AFROX gases, South Africa) was used as a carrier gas for the synthesis of N-CNTs. Images of the synthesized N-CNTs were obtained by using scanning electron microscopy (SEM) (JOEL JEM 1010) and transmission electron microscopy (TEM) (JOEL JSM 6100). Higher magnification images of N-CNTs were obtained from high-resolution transmission electron microscope (HRTEM). Elemental analysis was conducted on a LECO CHNS elemental analyser. The crystallinity of the N-CNTs was determined with a Rigaku/D_{max} RB powder X-ray diffractometer using graphite monochromatized high-density Cu Kα radiation (λ= 0.15406). The thermal stabilities of N-CNTs were determined using a Q Series^{TM} Thermal Analyzer TGA/DSC (Q600). The Fourier transform infrared (FTIR) spectra of N-CNTs were recorded on a PerkinElmer Spectrum RX1 FTIR spectrometer by embedding the samples into KBr pellets. The adsorption-desorption isotherms and surface area of N-CNTs were determined on a Micrometrics Tristar II surface area analyser. The graphitic nature of the N-CNTs was determined by a Raman spectrometer (DeltaNu Advantage 532^{TM}). Four accumulated spectra were collected to access the homogeneity of the samples. The synthesized N-CNTs were purified in nitric acid under microwave irradiation using a CEM Discover SP microwave instrument. The surface chemical composition of N-CNTs was analysed using X-ray photoelectron spectroscopy (XPS). XPS analysis was conducted on a Quantum 2000 instrument using a monochromated Al Kα source and charge neutralizer, with a pass energy of 117.4 eV. The peaks were deconvoluted using CasaXPS programme. The surface charge on the N-CNTs in ultra-pure water was determined with a Malvern Zetasizer (NS500). Boehm titration was conducted to quantify the acidic functional groups on the N-CNT surfaces. Potassium hydrogen phthalate (KHP) was used as the primary standard for the standardization of NaOH solutions using phenolphthalein as the indicator [42]. 0.20 g of each N-CNTs samples were placed in separate bottles. 25 mL NaOH (0.05 M), Na_2CO_3 (0.025M) and $NaHCO_3$ (0.05 M) were added to the bottle, sealed and shaken for 24 h. The solutions were then filtered and titrated against standardized HCl or NaOH [43]. Different functional groups (i.e. phenolic, carboxylic, lactonic and hydroxyl groups) were calculated based on the amount of acid or base consumed.

2.2. Synthesis of 1-ferrocenylmethyl(2-methylimidazole) ($FcMeCH_3$)

The general procedure described by Pan *et al.* [44] was used to synthesize $FcMeCH_3$. Briefly, ferrocenemethanol (1 mM) and 2-methyl-1H-imidazole (1.1 mM) was refluxed in acetic acid for 9 h at 60 °C. The product formation was monitored using preparative TLC plates with a solvent system of CH_2Cl_2/MeOH (4:1). The product was neutralized with 50% KOH in distilled water to remove the acetic acid and then puried by column chromatography. The final product was washed in Na_2SO_4 and finally dried under vacuum to obtain yellow crystals. Detailed characterization of $FcMeCH_3$ has been reported in our previous work [45].

2.3. Synthesis of N-CNTs

N-CNTs were synthesized by pyrolyzing $FcMeCH_3$ catalysts in acetonitrile at 850 ^{o}C using the CVD method. In the experiment, different concentrations of benzophenone were added to the reaction mixture to study the effect of oxygen on the growth of N-CNTs. The CVD procedure and set-up described by Oosthuizen *et al*. [46] was followed. Briefly, 0.25 g of the catalyst was added to 0.5, 1.0, 1.5 and 2.0 g of benzophenone to produce 1, 2, 3 and 4 wt.% oxygen, respectively. The mixture was dissolved in acetonitrile (as carbon and nitrogen source) to make a 10 g solution . The reactant mixture was injected using a syringe at 0.8 mL min^{-1} through the quartz tube placed in a muffle furnace. The mixture was swept through the tube by 10% hydrogen in argon carrier gas for 100 mL min^{-1}. After 30 min of reaction, the furnace was allowed to cool to room temperature, and the product was collected from the hot region of the furnace**.** N-CNTs from 1-4 wt.% oxygen is denoted as N-CNTs-1%, N-CNTs-2%, N-CNTs-3% and N-CNTs-4%, respectively. N-CNTs-0% was synthesised by dissolving $FcMeCH_3$ catalyst in acetonitrile. For comparison, N-CNTs-Fe was synthesized using ferrocene and toluene as catalyst and solvent, respectively.

2.4. Purification procedure for N-CNTs

N-CNTs were purified using microwave digestion. Briefly, N-CNTs (0.8 g) were dispersed in nitric acid (6 M) by ultrasonic agitation for 45 min. After sonication, each sample was purified by a microwave assisted irradiation. This was done by placing 50 mL of the dispersed sample in a thermal resistant Teflon (Milestone (TFM)) vessel on a sample rotor available for 4 vessels. The microwave was set at 100 W power and ramped from room temperature to 100 ^{o}C for 30 min. After digestion, the obtained suspension was filtered on 0.1 μm PTFE membrane. The collected solid samples were washed with deionized water until a neutral pH was obtained. Afterwards, the N-CNTs were washed with alcohol and dried in an oven at 100 °C for 24 h.

3. Results and discussion

3.1. TEM analysis

The morphology of N-CNTs was studied by TEM. The obtained images are shown in Figure 1. The incorporation of nitrogen correlated with the bamboo-like structure typical of N-CNTs [47] (Figure 1a-f). The use of $FcMeCH_3$ as a catalyst in acetonitrile and benzophenone gave mainly clean N-CNTs (Figure 1) and in good yield (Table 1). This could be attributed to the cleaning effect of oxygen as it reacts with amorphous carbon to form CO_2. N-CNTs and carbon sphere (CS) are obtained in toluene solvent.

Table 1. Summary of the effect of oxygen from benzophenone on the yield of N-CNTs synthesized by using 1-ferrocenylmethyl[2-methylimidazole] catalyst in acetonitrile at 850 °C

Samples	Yield (%)
N-CNTs-0%	74
N-CNTs-1%	68
N-CNTs-2%	63
N-CNTs-3%	61
N-CNTs-4%	58

The N-CNTs yields decrease as the concentration of oxygen increases due to the formation of CO_2 from unreacted carbon and oxygen. The TEM images of N-CNTs-1% and N-CNTs-2% (Figure 1a and b) showed a curly tubular structure. This could be as a result of Fe catalyst left inside the N-CNTs with smaller diameters [48]. The bamboo compartment of N-CNTs-1%, N-CNTs-2%, N-CNTs-3% and N-CNTs-4% decreased as the concentration of oxygen increased (Table reftab2). All N-CNTs obtained are opened at the tips, while some region along the tube gave stacked cup-like cones. This suggests that the bamboo structures were obtained by tip growth mechanism [49]. The cup-like cones appear to be more prominent as the oxygen concentrations increased (Figure 1c and e). N-CNTs-0% and N-CNTs-Fe exhibit relatively straight tubes and a wall thickness of ∼15 nm. The wall thickness decreases as the concentration of oxygen from benzophenone increases (Table 2). This is due to a reduction in the number of corrugated carbon layers and the closure of tubes which resulted in reduced compartment distances [50].

Table 2 shows the effect of oxygen on the inner diameter (ID) and outer diameter (OD) of the synthesized N-CNTs. From the results, it is believed that oxygen plays a vital role in modulating the morphology and diameters of N-CNT [39]. The OD decrease as the oxygen content in the reaction mixtures increases. This is due to the effect of oxygen on the catalyst leading to a decrease in Fe particle size as a result of catalyst migration, sintering, and precipitation processes [51, 52]. It was suggested that oxygen enhances the catalyst activity by removing amorphous carbon which prevents N-CNTs surface

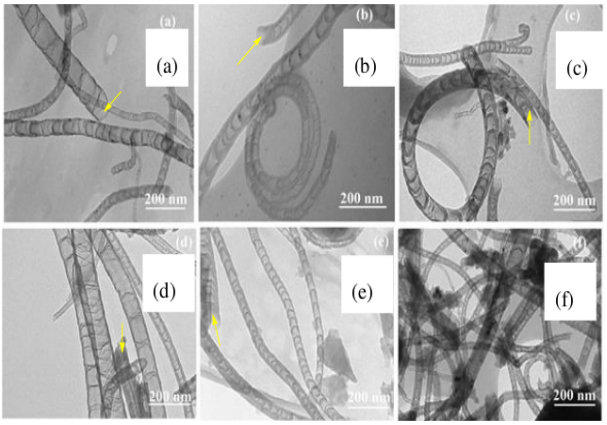

Figure 1. TEM images of N-CNTs obtained from (a) N-CNTs-0%, (b) N-CNTs-1%, (c) N-CNTs-2%, (d) N-CNTs-3%, (e) N-CNTs-4% and (f) N-CNTs-Fe

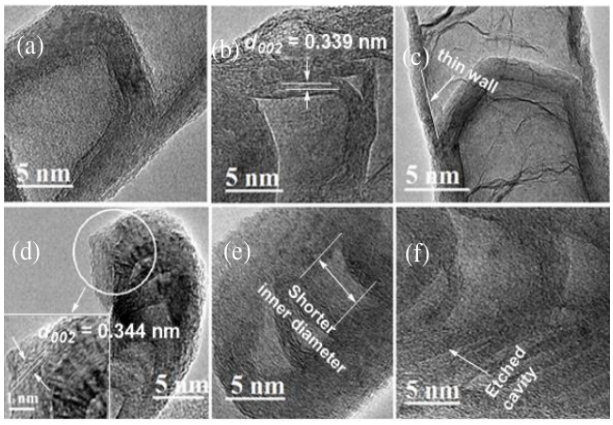

Figure 2. Eect of oxygen on N-CNT wall thickness and diameters: HRTEM images of (a) N-CNTs-0%, (b) N-CNTs-1%, (c) N-CNTs-2%, (d) N-CNTs-3%, (e) N-CNTs-4% and (f) etched wall of N-CNTs-4%

poisoning [41]. N-CNTs-1%, N-CNTs-2% and N-CNTs-3% gave smaller ID (14±7 nm to 16±5 nm). However, larger ID N-CNTs was obtained for N-CNTs-4% (i.e. 33±8 nm). This is due to excess oxygen content, leading to etching of the outer walls which largely affects N-CNTs quality.

Figure 2 shows the HRTEM images of N-CNTs with varying oxygen contents. An increase in the d_{002} interlayer spacing of the graphitic carbon was observed as the OD decreases. The interlayer *d*-spacing increased from 0.339 nm (N-CNTs-1%) (Figure 2b) to 0.344 nm (N-CNTs-3%) (Figure 2d). The increase in the d_{002} spacing is due to the curvature of smaller diameter N-CNTs and higher strain caused by the structural defect on the nanotube walls [53]. Also, the regular bamboo compartment for N-CNTs-4% (Figure 2f) was destroyed. This is attributed to supersaturation of molten Fe catalyst particles with carbon [54]. It could also be as a result of highly reactive oxygen at the surface or within the molten Fe nanoparticles which form FeO (i.e. Fe + O_2 →FeO + O), leading to etching of the graphitic carbon.

3.2. SEM analysis

The morphology of N-CNTs was analysed using SEM. The obtained images are shown in Figure 3 (a-f). Figure 3 a-e manifested the effect of oxygen on N-CNTs growth and alignment. This was as a result of the reaction of oxygen with very reactive hydrogen radical involved in the hydrocarbon-based growth of nanotubes [20]. This helps to scavenge unreactive hydrogen which inhibits the growth of sp^2 like graphitic sheets [30]. For example, the vertical alignment was observed for N-CNTs-1%, N-CNTs-2% and N-CNTs-3% (Figure 3 b-d) compared to N-CNTs-Fe (Figure 3f) The alignment was depleted at higher oxygen concentration (as observed in N-CNTs-4%). This could be attributed to the partial oxidization Fe-catalyst which reduced catalyst density, leading to reduced N-CNTs nucleation [55].

At moderate oxygen concentration (i.e. N-CNTs-2%), the nanotubes walls are free of amorphous carbon (Figure 3c) as compared to N-CNTs-4% (Figure 3e) with more amorphous carbon and lesser tubes (Table 1).

3.3. Thermal studies

The thermal stabilities of N-CNTs with different oxygen wt.% loading was studied as shown in Figure 4. TGA analysis was measured in air at 25-1000 °C to give an idea of the oxygen content and the purity of the samples. The first mass loss due to loss of water appears before 100 °C. N-CNTs-1% shows a significant weight loss at 386 °C while N-CNTs with 2-4 wt.% oxygen showed a weight loss between 390-530 °C. N-CNTs-0% is the most thermally stable with the decomposition temperature at 589 °C. The oxygen treated N-CNTs started to decompose at the on-set point between 334 and 430 °C (Table 3). All N-CNTs showed weight loss after decomposition above 87% with a residual mass between 9.6-0.5%. From DTG curves, the maximum mass loss temperature for 1-4% oxygen-treated N-CNTs is between 392 and 514 °C. Further investigation by Raman, XPS and FTIR analysis was done.

3.4. Crystallinity of N-CNTs

Figure 5 shows the Raman spectra of N-CNTs-0%, N-CNTs-1%, N-CNTs-2%, N-CNTs-3%, N-CNTs-4% and N-CNTs-Fe. The two prominent peaks observed at ~1330 and ~1573 cm^{-1} are assigned to the D- and G-bands, respectively. The intensity ratios of the D- and G-bands (I_D/I_G) shows the defect level of graphitic carbon materials [56, 57, 58]. The I_D/I_G ratio of N-CNTs-0% and N-CNT-Fe is 0.74 and 0.66, respectively (Table 4). After introduction of oxygen from benzophenone in the reactant precursor, the I_D/I_G ratio increased to 0.97, 0.93, 0.85 and 0.79 for N-CNTs-1%, N-CNTs-2%, N-CNTs-3% and N-CNTs-4%, respectively. This is as a result of incorporation of surface

Table 2. Effect of oxygen on N-CNTs diameter and wall thickness

Oxygen wt. %	Ave. OD±SD (nm)	Ave. ID±SD (nm)	Wall thickness (nm)	Ave. Compartment distance (nm)	N-CNTs (%)
N-CNTs-0%	48±25	38±31	15	18±11	90
N-CNTs-1%	37±31	19±5	11	17±9	85
N-CNTs-2%	33±21	14±7	9	15±8	76
N-CNTs-3%	34±19	16±5	8	13±9	74
N-CNTs-4%	41±15	33±8	7	11±8	65
N-CNTs-Fe	75±16	48±12	14	20±12	83

Table 3. Thermal features of N-CNTs at different oxygen concentration. $T_{oxidation}$ - refers to the temperature of primary oxidation.

Entry	Catalyst	On set point (^oC)	$T_{oxidation}$ (^oC)
1	N-CNTs-0%	430	572
2	N-CNTs-1%	378	450
3	N-CNTs-2%	397	410
4	N-CNTs-3%	346	428
5	N-CNTs-4%	334	420, 514
6	N-CNTs-Fe	386	392

Table 4. I_G/I_D ratios of the N-CNTs

Samples	D	G	I_D/I_G
N-CNTs-0%	1341	1591	0.74
N-CNTs-1%	1342	1601	0.97
N-CNTs-2%	1354	1599	0.93
N-CNTs-3%	1365	1595	0.85
N-CNTs-4%	1369	1590	0.79
N-CNT-Fe	1374	1581	0.66

oxygen functionalities and N atoms which produces more defects and disorders on the graphitic structure of the N-CNTs. The lower I_D/I_G ratio in N-CNT-Fe and N-CNTs-0% indicates that fewer defects are introduced in the carbon lattices due to less nitrogen atom intrusion into the graphitic carbon network compared to N-CNTs-1%, N-CNTs-2% and N-CNTs-3%, respectively. The width of the G-band peak also indicates the level of doping in N-CNTs [59, 60]. Table 4 shows that the G-band width of N-CNTs with varying concentrations of oxygen follows the order of N-CNTs-1% > N-CNTs-2% > N-CNTs-3% > N-CNTs-4% > N-CNTs-0% > N-CNTs-Fe. This result suggested a possible increase in N-doping at lower oxygen concentration.

3.5. Surface chemistry of N-CNTs

Figure 6 shows the FTIR spectra of N-CNTs from 0-4% of oxygen and N-CNTs-Fe. Peaks at around 2927 and 2625 cm^{-1} are assigned to the O–H and CH_3 stretching vibrations [61], respectively. The prominent band at 2381 cm^{-1} is assigned to the characteristic absorbance of CO_2 groups [62], while peaks at 1763, 1567 and 1030 cm^{-1} are assigned to stretching vibrations of C=O, C=N and C-O functional groups, respectively [63]. The peaks at 1375 cm^{-1} are assigned to stretching vibrations of C-NH_3 [64]. The presence of C=N and C-N functional group on the purified N-CNTs indicates the substitution of graphitic sp^2 carbon with nitrogen, leading to the bamboo configuration observed in TEM images [65]. For N-CNTs-0%, the intensity of the C=O band peak at 1763 cm^{-1} was weaker than that from 1-4% oxygen, which becomes broader as the concentration of

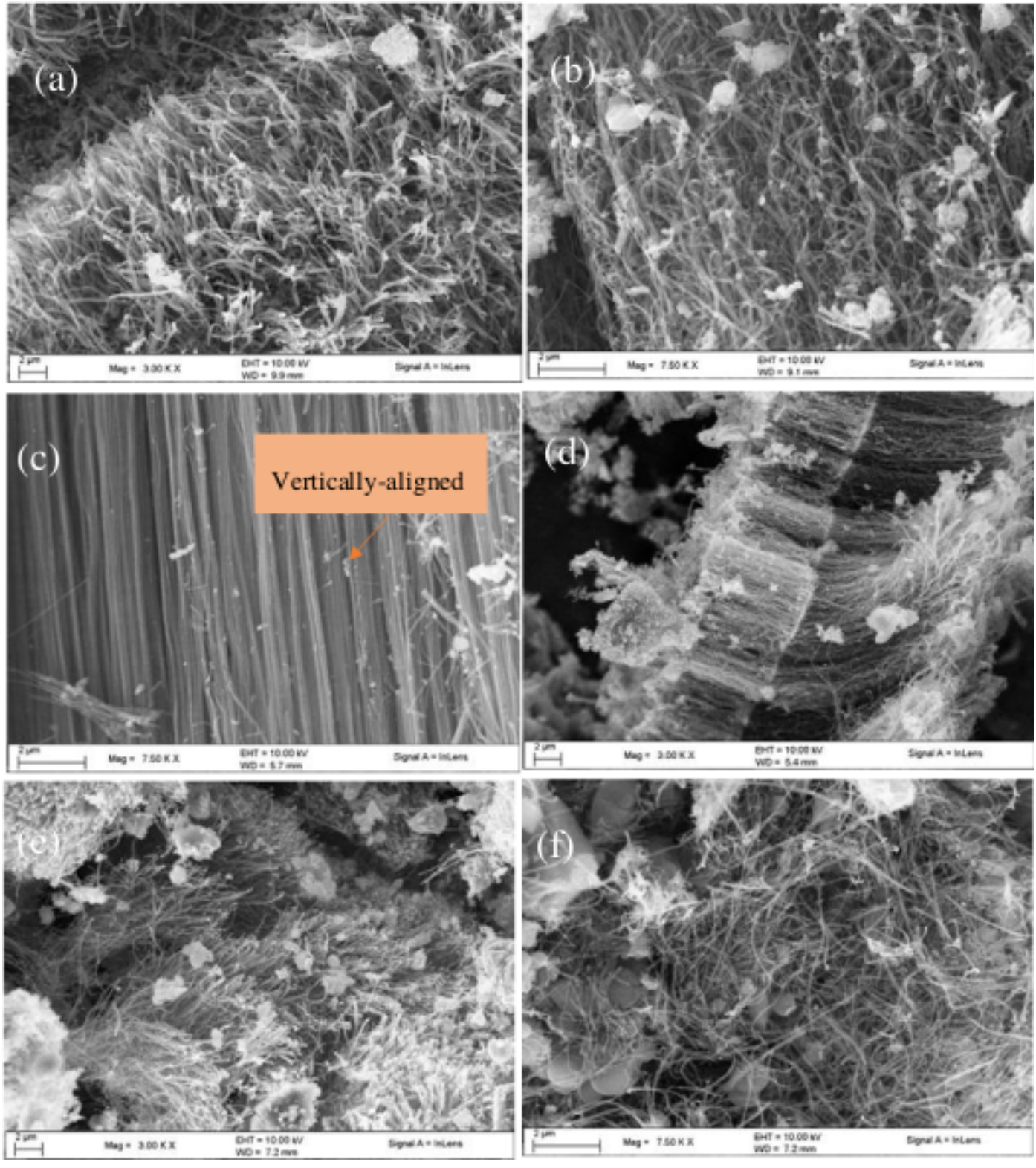

Figure 3. SEM images of (a) N-CNTs-0%, (b) N-CNTs-1%, (c) N-CNTs-2%, (d) N-CNTs-3%, (e) N-CNTs-4% and (f) N-CNTs-Fe

oxygen increases. The increase in the intensity of the C=N peak at 1567 cm^{-1} for N-CNTs from 1-4% oxygen can be related to the increase in nitrogen-doping level, which correlates with Raman analysis results (Table 4). The results of Boehm titration of N-CNTs-0%, N-CNTs-1%, N-CNTs-2%, N-CNTs-3%, N-CNTs-4% and N-CNTs-Fe are shown in Table 5. According to this method, $NaHCO_3$, Na_2CO_3 and NaOH, neutralize carboxyl groups, carboxyl groups and lactones; and carboxyl groups, lac-

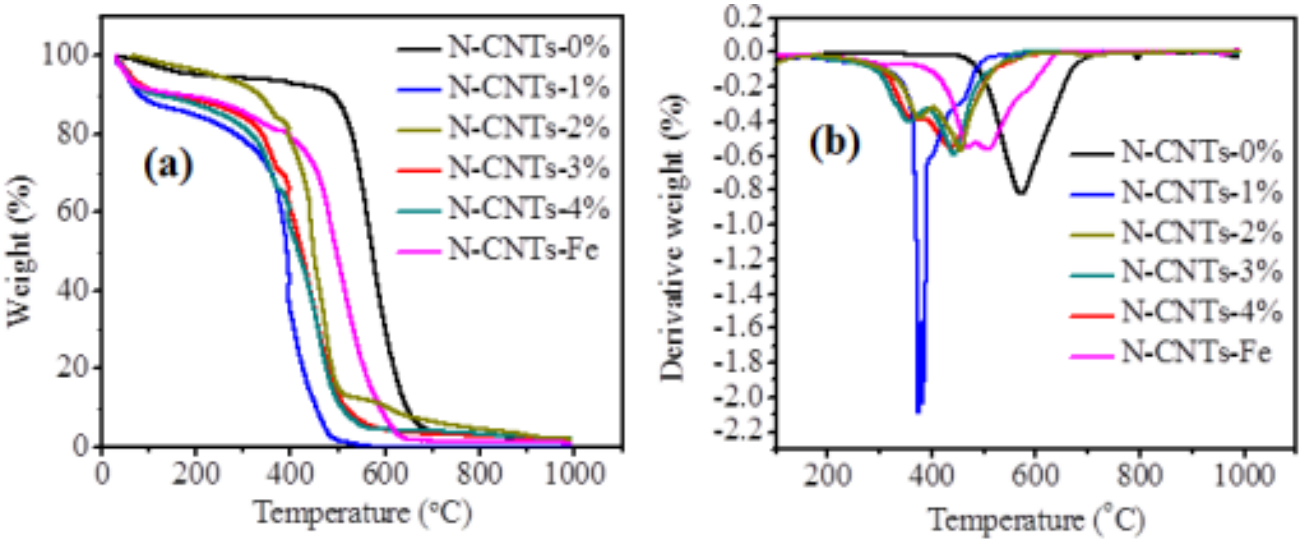

Figure 4. (a) TGA curves and (b) DTA of purified N-CNTs synthesized from 0-4% wt. oxygen

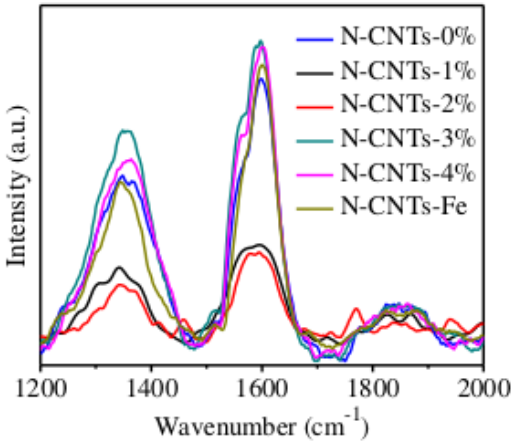

Figure 5. Raman spectra of N-CNTs

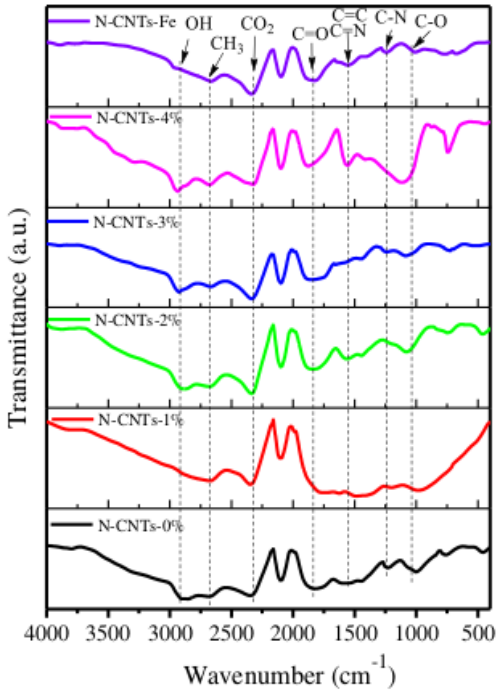

Figure 6. FTIR spectra of N-CNTs

tones and phenols, respectively. Therefore, different functional groups can be calculated from the volume of acid and bases used. The acid functional groups on N-CNTs-1%, N-CNTs-2%, N-CNTs-3% increases a little as the oxygen concentration increases compared to N-CNTs-0% and N-CNTs-Fe, while the amount of basic functional groups significantly increases. This indicates that the oxygen functionalities on the surface of N-CNTs synthesized in the presence of oxygen are more basic than N-CNTs synthesized in acetonitrile only [66]. From the results, N-CNTs-1%, N-CNTs-2%, N-CNTs-3% contains high concentration of basic group (≥ 1.025 mmol/g) (Table 5). Additionally, N-CNTs-2% has the highest concentration of the phenolic group.

Zeta potential (ζ) measurement provides information on the adsorption of ions (H^+ and OH^-) from aqueous suspension and dispersibility which lead to the formation of net charge on the N-CNTs [67]. These net charges lead to the formation of the electrical double layer which stabilizes the suspension and prevents particle aggregation. The properties of nanoparticles are largely affected by their colloidal stability. Nanoparticles with zeta potential less than -25 mV or above +25 mV are said to have a high degree of stability [67]. Table 6 shows the variation in the zeta potential of N-CNTs-0%, N-CNTs-1%, N-CNTs-2%, N-CNTs-3%, N-CNTs-4% and N-CNTs-Fe nanofluids. Our result showed that the zeta potential follows the

Table 5. Boehm titration of N-CNTs

Samples	Acidic groups (mmol/g)			Basic groups (mmol/g)
	Phenolic	Carboxylic	Lactonic	
N-CNTs-0%	0.766	0.813	0.070	0.889
N-CNTs-1%	0.085	1.025	0.680	1.025
N-CNTs-2%	0.181	1.142	0.0826	1.542
N-CNTs-3%	0.062	0.851	0.348	1.416
N-CNTs-4%	0.016	0.664	0.529	0.784
N-CNTs-Fe	0.0860	0.612	0.481	0.741

Table 6. Zeta potentials of N-CNTs in ultrapure water

Samples	Zeta potential (mV)
N-CNTs-0%	-37.6
N-CNTs-1%	-51.4
N-CNTs-2%	-57.0
N-CNTs-3%	-54.0
N-CNTs-4%	-43.2
N-CNTs-Fe	-38.8

Table 7. BET surface area and pore volume of N-CNTs-0%, N-CNTs-1%, N-CNTs-2%, N-CNTs-3%, N-CNTs-4% and N-CNTs-Fe

Samples	Surface area (m^2g^{-1})	Pore volume ($cm^3\ g^{-1}$)
N-CNTs-0%	95	0.37
N-CNTs-1%	127	0.35
N-CNTs-2%	130	0.57
N-CNTs-3%	122	0.53
N-CNTs-4%	89	0.39
N-CNTs-Fe	110	0.46

order N-CNTs-2% > N-CNTs-1% > N-CNTs-3% > N-CNTs-Fe > N-CNTs-0% > N-CNTs-4%. The zeta potential increases as the concentration of oxygen increases but drops sharply at higher oxygen concentration. According to this measurement, the oxidized N-CNTs are negatively charged in the aqueous phase as a result of oxygen-containing functional group ionization [68].

The effect of oxygen on the porosity of N-CNTs-0%, N-CNTs-1%, N-CNTs-2%, N-CNTs-3% and N-CNTs-4% was characterized by BET analysis. The nitrogen-adsorption isotherms of all N-CNTs are of type IV with different hysteresis loops in the high-pressure regions (P/P_o = 0.7–1), suggesting the presence of mesoporous structure [69]. As shown in Table 7, the surface areas of N-CNTs follows the order: N-CNTs-2% > N-CNTs-1% > N-CNTs-3% > N-CNTs-Fe > N-CNTs-0% > N-CNTs-4%. This indicates that the surface area of the N-CNTs can be modified by the introduction of oxygen into the reactant mixture.

3.6. Elemental analysis

The elemental composition and the bonding environment of the C, O and N species were determined by XPS analysis, and the result is presented in Table 8. Figure 7 shows the high-resolution N 1s energy region of selected N-CNTs (N-CNTs-0%, N-CNTs-3%, and N-CNTs-Fe). The deconvolution of the spectra gave three distinct N 1s peaks centred at 398.50, 400.18 and 401.20 eV assigned to pyridinic, pyrrolic and graphitic nitrogen, respectively [70]. A steady increase in the level of nitrogen-doping was observed during the CVD synthesis, followed by a gradual decrease due to an increase in oxygen con-

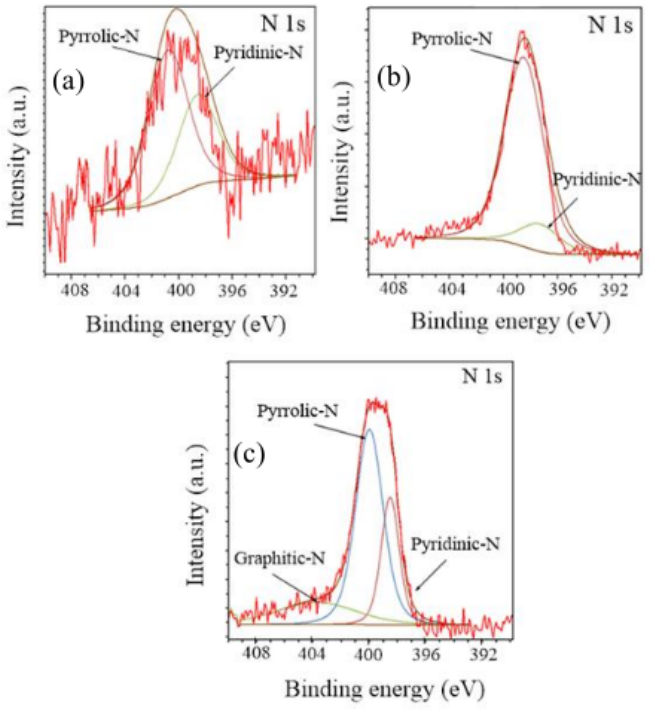

Figure 7. XPS N 1s spectra of (a) N-CNTs-0%, (b) N-CNTs-3% and (c) N-CNTs-Fe

centration (Table 8); a result consistent with Raman and TGA data. Compared with N-CNTs-0% and N-CNTs-Fe, the N-CNTs-3% gave higher pyrrolic-nitrogen species which could be attributed to the presence of active site caused by the lower amount of oxygenated species on the graphitic carbon framework [71]. At a low oxygen concentration in benzophenone, pyridinic-N species was formed (Table 8). At a high oxygen content, pyrrolic-N was obtained [72]. This may be due to the change in the elemental ratio (C: N: O) in the precursor mixture. The amount of nitrogen incorporated into N-CNTs obtained in our study is higher compared to other studies [34, 73]. This was attributed to the higher amount of nitrogen contained in the ferrocenyl imidazolium catalyst. Additionally, the decrease in nitrogen content could be ascribed to the presence of O in benzophenone which we believe inhibits nitrogen incorporation into N-CNTs. Deconvolution of O 1s spectra of N-CNTs-0%, N-CNTs-3% and N-CNTs-Fe peaks gave two bands centred at 531.26 and 533.40 eV assigned to C=O and C-O [74], respectively. The elemental analysis results (Table 8) corroborate XPS result with increased nitrogen-doping triggered by addition of varying amount of oxygen.

Table 9 shows the detailed analysis of C 1s peaks of N-CNTs-0%, N-CNTs-3% and N-CNTs-Fe. The deconvoluted C 1s peaks produced five components at 284.3, 285.8, 287.0, 287.9 and 289.4 eV, assigned to C=C, C-C, hydroxyl, carbonyl and carboxyl functional groups, respectively [75, 76]. From the

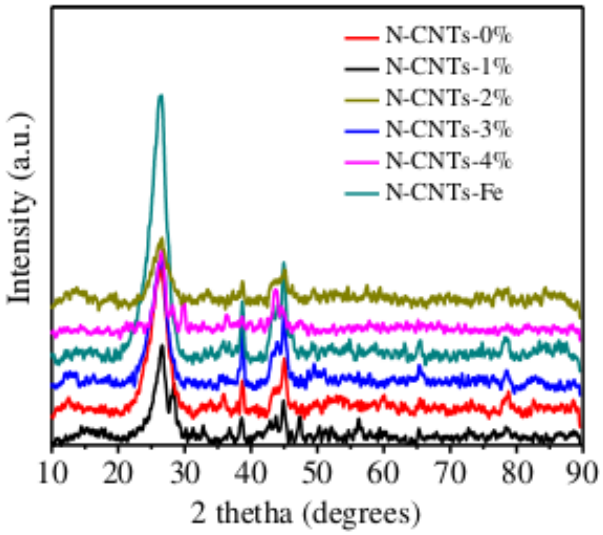

Figure 8. XRD patterns of the N-CNTs

XPS analysis, the carboxyl and carbonyl functional groups increase as the sp^2 carbon decreases. For example, the atomic percentage of C=O increased from 3.8 (N-CNTs-0%) to 8.8% (N-CNTs-3%). The oxidation of C=C is confirmed by an increase in C-C components, which led to the formation of new functional groups on N-CNT surfaces.

3.7. *Powder XRD pattern studies*

The XRD profiles of N-CNTs (i.e. 0-4 wt.% oxygen) and N-CNTs-Fe showed the crystalline nature of N-CNTs (Figure 8). All diffraction patterns showed the formation of (002) crystalline carbon plane (i.e. 26°), indicative of CNTs formation [77]. Other peaks at 44.5°, 49.1° and 77.6° correspond to (100), (221) and (401) reflections of the graphite structure of N-CNTs, respectively. The weak peaks at 37.6° and 43.5° are assigned to Fe_3C and Fe_2O_3, respectively, which are stuck inside the core of N-CNTs [78, 79]. The XRD diffraction pattern for N-CNTs showed a decrease in the intensities of (002) peaks as the alignment increases, particularly, from N-CNTs-1% to N-CNTs-3%. Also, the diffraction peak intensities of the (002) plane for N-CNTs-1%, N-CNTs-2% and N-CNTs-3% are weaker than those of N-CNTs-0% and N-CNTs-Fe. This shows that N-CNTs-Fe and N-CNTs-0% have fewer structural defects since N-doping create faults in the graphitic layers. This result agrees with the Raman results (Table 4). The interlayer *d*-spacing increases from 0.339 to 0.352 nm as oxygen concentration increases (Table 10). The increase in the d_{002} spacing is due to curvature of smaller diameter N-CNTs and higher strain caused by the structural defect on the nanotube walls. This result is consistent with d_{002} spacing obtained from HRTEM analysis.

Table 8. Relative atomic concentration and nitrogen species distribution from elemental and XPS analysis

	Elemental analysis			XPS analysis						
Samples	C (at.%)	O (at.%)	N (at.%)	C (at.%)	O (at.%)	N (at.%)	Pyrrolic (at.%)	Pyridinic (at.%)	Graphitic (at.%)	Nitrogen molecule (at. %)
N-CNTs-0%	80.36	11.62	8.02	72.72	8.36	9.92	8.60	2.30	0.70	0.30
N-CNTs-3%	71.82	13.04	15.14	77.00	9.40	13.36	11.80	1.24	0.80	0.20
N-CNTs-Fe	79.35	15.35	7.30	84.54	7.72	8.27	7.50	0.27	0.60	0.10

Table 9. Intensities of C 1s peaks

Samples	284.3 eV	285.8 eV	287.0 eV	287.9 eV	289.4 eV
	C=C sp^2 (%)	C-C sp^3 (%)	C-O (%)	C=O (%)	COOH (%)
N-CNTs-0%	75.5	5.9	13.6	3.8	1.2
N-CNTs-3%	75.3	4.7	11.4	8.8	0.8
N-CNTs-Fe	76.9	4.2	14.8	2.5	1.6

Table 10. X-ray structural parameters of N-CNTs-0%, N-CNTs-1%, N-CNTs-2%, N-CNTs-3%, N-CNTs-4% and N-CNTs-Fe. d_{002} values are obtained from HRTEM and correlated with those from the XRD analysis

Entry	Samples	d_{002} values (nm)	Intensity of C_{002} peaks	FWHM at C_{002} peaks	Crystalline size (nm)
1	N-CNT-Fe	0.348	488.41	2.446	3.06
2	N-CNT-0%	0.333	181.49	1.461	1.17
3	N-CNT-1%	0.339	129.72	1.548	1.41
4	N-CNT-2%	0.340	256.25	2.400	2.54
5	N-CNT-3%	0.344	247.13	2.616	2.61
6	N-CNT-4%	0.352	185.92	2.637	1.91

4. Conclusion

This study presented the role of oxygen and nitrogen-doping as a promising method to improve the physicochemical properties of N-CNTs. This has critical implications for reproducibility in N-CNT synthesis, particularly on the effect of oxygen in diameter and wall thickness control. It can be concluded that the introduction of an appropriate amount of oxygen promotes N-CNTs growth with clean walls and reduced diameters. From XPS analysis, pyrrolic-N was predominantly incorporated into the crystalline CNT structure at a high oxygen concentration. Nitrogen-doping was further confirmed by TGA analysis and Raman spectroscopy. Lastly, the understanding of the effect of oxygen species on the morphology and surface area of N-CNTs during synthesis is critical in vast numbers of industrially promising supported metal nanoparticles catalyst design.

Acknowledgments

This research was financially supported by the National Research Foundation (NRF) South Africa. We are grateful to the School of Chemistry and Physics, University of KwaZulu-Natal (UKZN) for creating a conducive research laboratory for this work. Ayomide is grateful to Prof. Vincent Nyamori, Prof.

Bernand Omondi and Mrs Rashidat Labulo for proofreading this manuscript.

References

[1] J. Zhang, X.B Yi, S. Liu, H.L Fan, W. Ju, Q.C & W. J. Ma, "Vertically aligned carbon nanotubes/carbon fibre paper composite to support Pt nanoparticles for the direct methanol fuel cell application", J Phys Chem Solids **102** (2017) 99.

[2] W. Li, C. Liang , J. Qiu, W. Zhou, H. Han, Z. Wei, G. Sun & Q. Xin, "Carbon nanotubes as support for cathode catalyst of a direct methanol fuel cell", Carbon **40** (2002) 787.

[3] Z. Bo, D. Hu, J. Kong, J. Yan & K. Cen, "Performance of vertically oriented graphene supported platinum-ruthenium bimetallic catalyst for methanol oxidation", J Power Sources **273** (2015) 530.

[4] S. Hong, J. Lee, K. Do, M. Lee, J.H Kim, S. Lee & D.H Kim, "Stretchable electronics: Stretchable electrode based on laterally combed carbon nanotubes for wearable energy harvesting and storage devices", Adv Funct Mater **27** (2017) 1770285.

[5] E. Titus, M.K Singh, G. Cabral, V. Paserin, P.R. Babu, W.J. Blau, J. Ventura, J.P. Araujo & J. Gracio, "Fabrication of vertically aligned carbon nanotubes for spintronic device applications", J Mater Chem **19** (2009) 7216.

[6] B-J. Lee & G-H, "Jeong Efficient surface functionalization of vertically-aligned carbon nanotube arrays using an atmospheric pressure plasma jet system", Fuller Nanotub Car N **26** (2018) 116.

[7] T. Tsai, C. Lee, N. Tai & Tuan W, "Transfer of patterned vertically aligned carbon nanotubes onto plastic substrates for flexible electronics and field emission devices", Appl Phys Lett **5** (2009) 013107.

[8] S. Ahadian, U. Naito, V.J. Surya, S. Darvishi, M. Estili, X. Liang, K. Nakajima, H. Shiku, Y. Kawazoe & T. Matsue, "Fabrication of poly (ethylene glycol) hydrogels containing vertically and horizontally aligned graphene using dielectrophoresis: An experimental and modelling study", Carbon **123** (2017) 460.

[9] N. Zhao, Z. Ma, H. Song, Y. Xie & M. Zhang Enhancement of bioelectricity generation by synergistic modification of vertical carbon nanotubes/polypyrrole for the carbon fibres anode in a microbial fuel cell. Electrochim Acta. **296** (2018) 69.

[10] W. Yang, Thordarson P, J.J Gooding, S.P Ringer & F. Braet, "Carbon nanotubes for biological and biomedical applications", Nanotechnol **18** (2007) 412001.

[11] H. Chen, A. Roy, J-B. Baek, L. Zhu, J. Qu & L. Dai, "Controlled growth and modification of vertically-aligned carbon nanotubes for multifunctional applications", Mater Sci Eng: R: Rep **70** (2010) 63.

[12] S.N Kim, J.F. Rusling & F. Papadimitrakopoulos, "Carbon nanotubes for electronic and electrochemical detection of biomolecules", Adv Mater **19** (2007) 3214.

[13] L.K. Putri, B.J Ng, W-J. Ong, H.W Lee, W.S Chang & S.P Chai, "Heteroatom nitrogen-and boron-doping as a facile strategy to improve photocatalytic activity of standalone reduced graphene oxide in hydrogen evolution", ACS Appl Mater Interface **9** (2017) 4558.

[14] W. Han, Y. Bando, K. Kurashima & T. Sato, "Boron-doped carbon nanotubes prepared through a substitution reaction", Chem Phys Lett **299** (1999) 368.

[15] V. Perazzolo, E. Gradzka, C. Durante, R. Pilot, N. Vicentini, G.A. Rizzi, G. Granozzi & A. Gennaro, "Chemical and electrochemical stability of nitrogen and sulphur doped mesoporous carbons", Electrochim Acta **197** (2016) 251.

[16] J.P. Paraknowitsch & A. Thomas, "Doping carbons beyond nitrogen: an overview of advanced heteroatom doped carbons with boron, sulphur and phosphorus for energy applications", Energy Env Sci **6** (2013) 2839.

[17] M.I. Ionescu, Y. Zhang, R. Li, H. Abou-Rachid & X. Sun, "Nitrogen-doping effects on the growth, structure and electrical performance of carbon nanotubes obtained by spray pyrolysis method", Appl Surf Sci **258** (2012) 4563.

[18] M. Scardamaglia, M. Amati, B. Llorente, P. Mudimela, J.F. Colomer, J. Ghijsen, C. Ewels, R. Snyders, L. Gregoratti & C. Bittencourt, "Nitrogen ion casting on vertically aligned carbon nanotubes: tip and sidewall chemical modification". Carbon **77** (2014) 319.

[19] J.F. Colomer, B. Ruelle, N. Moreau, S. Lucas, R. Snyders, T. Godfroid, C. Navio & C. Bittencourt, "Vertically aligned carbon nanotubes: synthesis and atomic oxygen functionalization", Surf Coatings Technol **205** (2011) S 592.

[20] A. Lopez-Bezanilla, "Electronic and quantum transport properties of substitutionally doped double-walled carbon nanotubes", J Phys Chem C **118** (2014) 1472.

[21] E.N Nxumalo & N.J. Coville,"Nitrogen-doped carbon nanotubes from organometallic compounds: A review", Mater **3** (2010) 2141.

[22] S. Van Dommele, A. Romero-Izquirdo, R. Brydson, K. De Jong & J. Bitter,"Tuning nitrogen functionalities in catalytically grown nitrogen-containing carbon nanotubes" Carbon **46** (2008) 138.

[23] C. Tang, Y. Bando, D. Golberg & F. Xu, "Structure and nitrogen incorporation of carbon nanotubes synthesized by catalytic pyrolysis of dimethylformamide", Carbon **42** (2004) 2625.

[24] T. Sugai, H. Yoshida, T. Shimada, T. Okazaki, H. Shinohara & S. Bandow, "New synthesis of high-quality double-walled carbon nanotubes by high-temperature pulsed arc discharge", Nano Lett **3** (2003) 769.

[25] S. Dixit, S. Singhal, V. Vankar & A. Shukla, "Size-dependent Raman and absorption studies of single-walled carbon nanotubes synthesized by pulse laser deposition at room temperature", Optical Mater **72** (2017) 612.

[26] B. McLean, C.A. Eveleens, I. Mitchell, G.B. Webber & A.J. Page, "Catalytic CVD synthesis of boron nitride and carbon nanomaterials–synergies between experiment and theory", Phys Chem Chem Phys **19** (2017) 26466.

[27] S.L. Pirard, S. Douven & J.P. Pirard, "Large-scale industrial manufacturing of carbon nanotubes in a continuous inclined mobile-bed rotating reactor via the catalytic chemical vapour deposition process", Front Chem Sci Eng **11** (2017) 280.

[28] M. Bansal, C. Lal, R. Srivastava, M. Kamalasanan & L. Tanwar, "Comparison of structure and yield of multiwall carbon nanotubes produced by the CVD technique and a water assisted method", Phys B: Condens Matter **405** (2010) 1745.

[29] G.D Nessim, A. Al-Obeidi, H. Grisaru, E.S. Polsen, C.R Oliver, T. Zimrin, A.J Hart, D. Aurbach & C.V Thompson, "Synthesis of tall carpets of vertically aligned carbon nanotubes by in situ generation of water vapour through preheating of added oxygen", Carbon **50** (2012) 4002.

[30] G. Zhang, D. Mann, L. Zhang, A. Javey, Y. Li, E. Yenilmez, Q. Wang, J.P. McVittie, Y. Nishi, J. Gibbons & H. Dai, "Ultra-high-yield growth of vertical single-walled carbon nanotubes: Hidden roles of hydrogen and oxygen", P Natl Aca Sci USA **102** (2005) 16141.

[31] T. Yamada, A. Maigne, M. Yudasaka, K. Mizuno, D.N. Futaba, M. Yumura, S. Iijima & K. Hata, "Revealing the secret of water-assisted carbon nanotube synthesis by microscopic observation of the interaction of water on the catalysts", Nano Lett **8** (2008) 4288.

[32] K. Hasegawa & S. Noda, "Millimeter-tall single-walled carbon nanotubes are rapidly grown with and without water", ACS Nano **5** (2011) 975-.

[33] Q. Wen, W. Qian, F. Wei, Y. Liu, G. Ning & Q. Zhang, "CO2-assisted SWNT growth on porous catalysts", Chem Mater **19** (2007) 1226.

[34] L.M.Ombaka, P.G. Ndungu & V.O. Nyamori, "Tuning the nitrogen content and surface properties of nitrogen-doped carbon nanotubes synthesized using a nitrogen-containing ferrocenyl derivative and ethyl benzoate", J Mater Sci **50** (2015) 1187.

[35] M.H. Rümmeli, F. Schäffel, C. Kramberger, T. Gemming, A. Bachmatiuk, R.J Kalenczuk, B. Rellinghaus, B. Büchner & T. Pichler, "Oxide-driven carbon nanotube growth in supported catalyst CVD", J Am Chem Soc **129** (2007) 15772.

[36] J.B. In, C.P. Grigoropoulos, A.A. Chernov & A. Noy, "Growth kinetics of vertically aligned carbon nanotube arrays in clean oxygen-free condi-

tions", ACS Nano **5** (2011) 9602.

[37] S. Sakurai, M. Yamada, K. Hata & D.N. Futaba, "Limitation in growth temperature for water-assisted single-wall carbon nanotube forest synthesis", MRS Adv **3** (2018) 91.

[38] D.N. Futaba, K. Hata, T. Namai, T. Yamada, K. Mizuno, Y. Hayamizu, M. Yumura & S. Iijima, "84% catalyst activity of water-assisted growth of single-walled carbon nanotube forest characterization by a statistical and macroscopic approach", J Phys Chem B **110** (2006) 8035.

[39] G.D. Nessim, A.J. Hart, J.S. Kim, D. Acquaviva, J. Oh, C.D. Morgan, M. Seita, J.S. Leib & C.V. Thompson, "Tuning of vertically-aligned carbon nanotube diameter and areal density through catalyst pre-treatment", Nano Lett **8** (2008) 3587.

[40] P.B. Amama, C.L. Pint, L. McJilton, S.M. Kim, E.A. Stach, P.T. Murray, R.H. Hauge & B. Maruyama, "Role of water in the super growth of single-walled carbon nanotube carpets", Nano Lett **9** (2008) 44.

[41] W. Shi, J. Li, E.S. Polsen, C.R. Oliver, Y. Zhao, E.R. Meshot, M. Barclay, D.H. Fairbrother, A.J. Hart & D.L. Plata, "Oxygen-promoted catalyst sintering influences number density, alignment, and wall number of vertically aligned carbon nanotubes", Nanoscale **9** (2017) 5222.

[42] H.P. Boehm, "Surface oxides on carbon and their analysis: A critical assessment", Carbon **40** (2002) 145.

[43] B. Petrova, B. Tsyntsarski, T. Budinova, N. Petrov, L.F. Velasco & C.O Ania, "Activated carbon from coal tar pitch and furfural for the removal of p-nitrophenol and m-aminophenol", Chem Eng J **172** (2011) 102.

[44] P. He, Y. Du, S. Wang, C. Cao, X. Wang, G. Pang & Y. Shi, "Synthesis, Structure, and Reactivity of Ferrocenyl-NHC Palladium Complexes", Z Anorg Allg Chem **639** (2013) 1004.

[45] A.H. Labulo, N.P. Ngidi, B. Omondi, V.O. Nyamori, "Physicochemical properties of nitrogen-doped carbon nanotubes from metallocenes and ferrocenyl imidazolium compounds", J Organomet Chem **868** (2018) 66.

[46] R.S. Oosthuizen & V.O. Nyamori, "Heteroatom-containing ferrocene derivatives as catalysts for MWCNTs and other shaped carbon nanomaterials", Appl Organomet Chem **26** (2012) 536.

[47] Q. Li, H. Pan, D. Higgins, R. Cao, G. Zhang, H. Lv, K. Wu, J. Cho & G. Wu, "Metal-organic framework-derived bamboo-like nitrogen-doped graphene tubes as an active matrix for hybrid oxygen-reduction electrocatalysts", Small **11** (2015) 1443.

[48] X. Zhao, F. Li, R. Wang, J.M. Seo, H.J. Choi, S.M. Jung, J. Mahmood, I.Y. Jeon & J.B Baek, "Controlled fabrication of hierarchically structured nitrogen-doped carbon nanotubes as a highly active bifunctional oxygen electrocatalyst", Adv Funct Mater **27** (2017) 1605717.

[49] R. Zhang, Y. Zhang & F. Wei, "Horizontally aligned carbon nanotube arrays: growth mechanism, controlled synthesis, characterization, properties and applications", Chem Soc Rev **46** (2017) 3661.

[50] B.G. Sumpter, J. Huang, V. Meunier, J.M. Romo-Herrera, E. Cruz-Silva, H. Terrones & M. Terrones, "A theoretical and experimental study on manipulating the structure and properties of carbon nanotubes using substitutional dopants", Int J Quantum Chem **109** (2009) 97.

[51] H. Okuyama, N. Iwata & H. Yamamoto, "Growth of vertically aligned carbon nanotubes depending on the thickness of catalyst films by plasma-enhanced chemical vapour deposition", Mol Cryst Liq Cryst **472** (2007) 209.

[52] Ç. Öncel & Y. Yürüm, "Carbon nanotube synthesis via the catalytic CVD method: A review of the effect of reaction parameters", Fuller Nanotub Car N **14** (2006) 17.

[53] S.I. Yengejeh, S.A. Kazemi & A. Öchsner, "Advances in mechanical analysis of structurally and atomically modified carbon nanotubes and degenerated nanostructures: A review", Compos Part B: Eng **86** (2016) 95.

[54] L. Zhou, L.R. Enakonda, M. Harb, Y. Saih, A. Aguilar-Tapia, S. Ould-Chikh, J.L. Hazemann, J. Li, N. Wei, D. Gary & P. Del-Gallo, "Fe catalysts for methane decomposition to produce hydrogen and carbon nanomaterials", Appl Catal B: Env **208** (2017) 44.

[55] E. Teblum, Y. Gofer, C.L. Pint & G.D. Nessim, "Role of catalyst oxidation state in the growth of vertically aligned carbon nanotubes", J Phys Chem C **116** (2012) 24522.

[56] J. Wang, M.J. Shea, J.T. Flach, T.J. McDonough, A.J. Way, M.T. Zanni & M.S. Arnold, "Role of defects as exciton quenching sites in carbon nanotube photovoltaics", J Phys Chem C **121** (2017) 8310.

[57] W. Xia, "Interactions between metal species and nitrogen-functionalized carbon nanotubes", Catal SciTechnol **6** (2016) 630.

[58] S,L. Rebelo, A. Guedes, M.E. Szefczyk, A.M. Pereira, J.P. Araújo & Freire C, "Progress in the Raman spectra analysis of covalently functionalized multiwalled carbon nanotubes: unravelling disorder in graphitic materials", Phys Chem Chem Phys **18** (2016) 12784.

[59] M.A. Pimenta, E. del Corro, B.R. Carvalho, C. Fantini & L.M. Malard, "Comparative study of Raman spectroscopy in graphene and MoS2-type transition metal dichalcogenides", Acc Chem Res **48** (2014) 41.

[60] X. Zhang, W.P. Han, X.F. Qiao, Q.H. Tan, Y.F. Wang, J. Zhang & P.H. Tan, "Raman characterization of AB-and ABC-stacked few-layer graphene by interlayer shear modes", Carbon **99** (2016) 118.

[61] X.Y. Yang, J.J. Xu, Z.W. Chang, D. Bao, Y.B. Yin, T. Liu, J.M. Yan, D.P. Liu, Y. Zhang & X.B Zhang, "Blood-capillary-inspired, free-standing, flexible, and low-cost super-hydrophobic N-CNTs@ SS cathodes for high-capacity, high-rate, and stable Li-ion batteries", Adv Energy Mater **8** (2018) 1702242.

[62] S. Nie, W. Wu, Y. Pan, X. Dong, B. Li & D.Y. Wang, "Studies on intumescent flame retardant polypropylene composites based on biodegradable wheat straw", Fire Mater. **42** (2018) 703.

[63] R. Rao, M. Yang, Q. Ling, C. Li, Q. Zhang, H. Yang & A. Zhang, "A novel route of enhancing oxidative catalytic activity: Hydroxylation of MWCNTs induced by sectional defects", Catal Sci Technol **4** (2014) 665.

[64] A. Ameli, M. Arjmand, P. Pötschke, B. Krause & U. Sundararaj, "Effects of synthesis catalyst and temperature on broadband dielectric properties of nitrogen-doped carbon nanotube/polyvinylidene fluoride nanocomposites. Carbon **106** (2016) 260.

[65] H. Liu, H. Hu, J. Wang, P. Niehoff, X. He, E. Paillard, D. Eder, M. Winter & J. Li, "Hierarchical ternary MoO2/MoS2/heteroatom-doped carbon hybrid materials for hig-performance lithium-ion storage", ChemElectroChem **3** (2016) 922.

[66] H.R. Barzegar, E. Gracia-Espino, T. Sharifi, F. Nitze & T. Waagberg, "Nitrogen doping mechanism in small diameter single-walled carbon nanotubes: impact on electronic properties and growth selectivity", J Phys Chem C **117** (2013) 25805.

[67] B. Pal, S.S. Mallick & B. Pal, "Anisotropic CuO nanostructures of different size and shape exhibit thermal conductivity superior to typical bulk powder. Colloids Surf A: Physicochem Eng Asp **459** (2014) 282.

[68] X. Peng, J. Jia, X. Gong, Z. Luan & B. Fan, "Aqueous stability of oxidized carbon nanotubes and the precipitation by salts", J Hazard Mater **165** (2009) 1239.

[69] N. Iqbal, X. Wang, J. Yu, N. Jabeen, H. Ullah & B. Ding, "In situ synthesis of carbon nanotube doped metal-organic frameworks for CO2 capture", RSC Adv **6** (2016) 4382.

[70] Z. Huang, Z. Liao, W. Yang, H. Zhou, C. Fu, Y. Gong, L. Chen & Y. Kuang, "Different types of nitrogen species in nitrogen-doped carbon material: The formation mechanism and catalytic role on oxygen reduction reaction", Electrochim Acta. **245** (2017) 957.

[71] Z-H. Sheng, L. Shao, J-J. Chen, W-J. Bao, F-B. Wang & X-H. Xia, "Catalyst-free synthesis of nitrogen-doped graphene via thermal annealing graphite oxide with melamine and its excellent electrocatalysis", ACS Nano **5** (2011) 4350.

[72] G. Bepete, ZN. Tetana, S. Lindner, M.H. Rümmeli, Z. Chiguvare & N.J. Coville, "The use of aliphatic alcohol chain length to control the nitrogen type and content in nitrogen-doped carbon nanotubes", Carbon **52** (2013).316.

[73] T.E. Bell, G. Zhan, K. Wu, H.C. Zeng & L. Torrente-Murciano, "Modification of ammonia decomposition activity of ruthenium nanoparticles by N-doping of CNT supports", Topics Catal **60** (2017) 1251.

[74] J. Yu, Y. Zhong, W. Zhou & Z. Shao, "Facile synthesis of nitrogen-doped carbon nanotubes encapsulating nickel-cobalt alloys 3D networks for oxygen evolution reaction in an alkaline solution", J Power Sources

338 (2017) 26.

[75] T. Okpalugo, P. Papakonstantinou, H. Murphy, J. McLaughlin & N. Brown, "High-resolution XPS characterization of chemical functionalised MWCNTs and SWCNTs", Carbon **43** (2005) 153.

[76] R. Ionescu, E.H. Espinosa, E. Sotter, E. Llobet, X. Vilanova, X. Correig, A. Felten, C. Bittencourt, G. Van Lier, J.C. Charlier & J.J. Pireaux, "Oxygen functionalisation of MWNT and their use as gas sensitive thick-film layers", Sens Actuators B: Chem **113** (2006) 36.

[77] A. Sharma, K. Dasgupta, S. Banerjee, A. Patwardhan, D. Srivastava & J.B. Joshi, "In-situ nitrogen doping in carbon nanotubes using a fluidized bed reactor and hydrogen storage behaviour of the doped nanotubes", Int J Hydrogen Energy **42** (2017) 10047.

[78] Z. Li, R. Liu, Y. Xu & X. Ma, "Enhanced Fischer-Tropsch synthesis performance of iron-based catalysts supported on nitric acid treated N-doped CNTs", Appl Surf Sci **347** (2015) 643.

[79] T .Fu, R. Liu, J. Lv & Z. Li, "Influence of acid treatment on N-doped multi-walled carbon nanotube supports for Fischer-Tropsch performance on cobalt catalyst", Fuel Process Technol **122** (2014) 49.